ACS OMEGA

http://pubs.acs.org/journal/acsodf

Article

Electrode-Integrated Textile-Based Sensors for In Situ Temperature and Relative Humidity Monitoring in Electrochemical Cells

Sadegh Hasanpour, Armin Rashidi, Tavia Walsh, Erik Pagan, Abbas S. Milani, Mohsen Akbari,* and Ned Djilali*

Cite This: *ACS Omega* 2021, 6, 9509−9519

Read Online

ACCESS | Metrics & More | Article Recommendations | Supporting Information

ABSTRACT: Temperature and humidity measurements in electrochemical energy devices are essential for maximizing their overall performance under different operating conditions and avoiding hazardous consequences that may arise from the malfunction of these systems. Using sensors for in situ measurements of temperature and relative humidity (RH) is a promising approach for continuous monitoring and management of electrochemical power sources. Here, we report on the feasibility of using thread-based sensors for in situ measurements of temperature and RH in proton exchange membrane fuel cells (PEMFCs) as an example of electrochemical energy devices. Commodity threads are low-cost and flexible materials that hold great promise for the creation of complex three-dimensional (3D) circuits using well-established textile methods such as weaving, braiding, and embroidering. Ex situ and in situ characterization show that threads can be introduced in the gas diffusion layer (GDL) structure to inscribe water highways within the GDL with minimal impact on the GDL microstructure and transport properties. Fluorinated ethylene propylene (FEP) is coated on thread-based sensors to decouple the response to temperature and humidity; the resulting threads achieve a linear change of resistance with temperature (−0.31%/°C), while RH is monitored with a second thread coated with poly(dimethylsiloxane) (PDMS). The combination of both threads allows for minimally invasive and dynamically responsive monitoring of local temperature and RH within the electrode of PEMFCs.

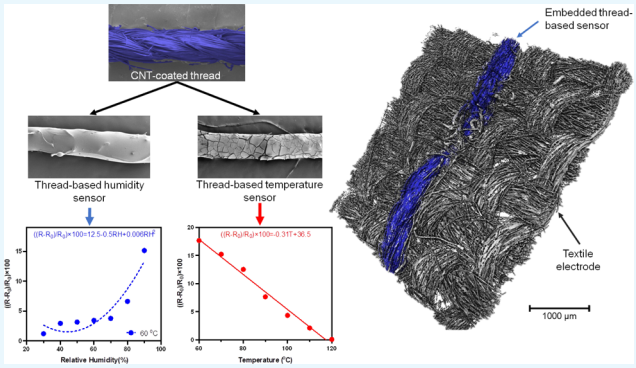

INTRODUCTION

Electrochemical energy conversion and storage technologies are central to the decarbonization of the transportation and power sectors. They provide the reliability and flexibility required to bring low-cost intermittent renewable energy sources into major energy-consuming sectors.[1] Porous electrodes are pivotal components in many electrochemical devices, such as polymer electrolyte membrane fuel cells (PEMFCs)[2] and redox-flow batteries.[3,4] Porous electrodes typically consist of a multilayered structure with multiscale pore sizes. Additionally, numerous studies have shown that the performance of electrochemical systems is strongly dependent upon the relative humidity (RH) of the environment and the electrochemical cell.[5,6] For example, controlling local overheat in lithium-ion batteries or PEMFCs is critical to preventing thermal runaway and its subsequent hazardous consequences such as fire and explosion.[7−9] Additionally, a balance between temperature and local humidity in PEMFCs is of utmost importance to ensure their high performance in various operating conditions and to maximize their life cycle.[10] The measurement of temperature and humidity within electrochemical power sources is crucial for monitoring these systems and managing their performances.

The temperature and humidity of electrochemical power sources can be determined by employing external measurement methods that include imaging by infrared cameras and installing sensors on the electrochemical cells' outer body. However, these measurement methods do not provide any information about the spatiotemporal distribution of temperature and RH within the electrochemical cells. Alternatively, in situ measurement techniques, such as micropatterned flexible sensors, optical-based sensors such as Fiber Bragg grating (FBG) sensors, and tunable diode laser absorption spectroscopy, have recently emerged for monitoring temperature and RH in electrochemical power sources.[11−15] Although these methods provide repeatable and reliable responses, their application for in situ monitoring of temperature and humidity is hampered by the need for expensive and labor-intensive micropatterning techniques to create thin-film microsensors on

Received: December 28, 2020
Accepted: February 24, 2021
Published: March 29, 2021

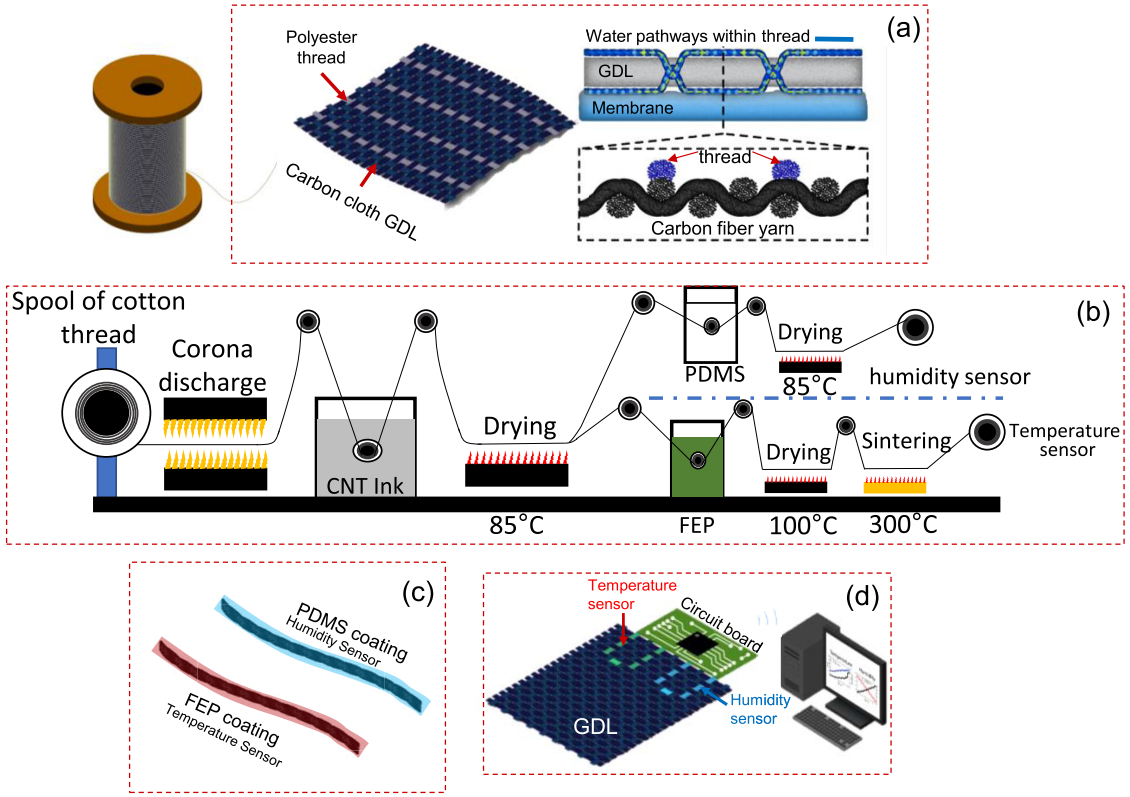

Figure 1. Schematic of the process to modify carbon cloth GDL via sewing hydrophilic and temperature- and humidity-sensing threads. (a) Polyester threads sewed on the carbon cloth GDL generating hydrophilic pathways for water removal. (b) Proposed roll-to-roll process of dip-coating cotton threads to confer humidity and temperature sensitivity. (c) FEP for temperature sensing and PDMS coating for humidity sensing. (d) Sewing of thread-based sensors for wireless monitoring of temperature and humidity.

the surfaces and challenges associated with the blockage of the optical path or sensing window for optical-based systems.

Commodity threads, traditionally used in the apparel industry, have recently emerged as an inexpensive material for creating flexible sensors. The wicking property and flexibility of threads make them promising candidates for creating complex three-dimensional (3D) circuits using well-established textile methods such as weaving, braiding, and embroidering. Additionally, using threads as green material helps with reducing global e-waste and chemical waste. Recently, Mostafalu et al. developed a multitude of physical and chemical sensors by infusing cotton threads with carbon nanotubes.[16] They used these sensors to measure biological quantities, including pH, temperature, and glucose, in small animals. Mousavi and co-workers developed thread-based potentiometric electrodes to detect physiological electrolytes selectively.[17] They demonstrated the application of these sensors in the analysis of ions in soil/water slurries and dietary supplements. In another study, Owyeung et al. developed highly flexible transistor threads for multiple diagnostic applications.[18] These sensors were used to measure multiple biological markers in multiple samples simultaneously. In the context of electrochemical power sources, Wang et al. recently developed a microfluidic fuel cell using nanoparticle-infused cotton threads as electrodes.[19] They showed that this low-cost system could generate power of tens of milliwatts per square centimeter, which is suitable for powering portable diagnosis devices. However, they did not report on using these threads for in situ temperature and humidity measurements.

In this work, we report on the feasibility of using thread-based sensors for in situ measurements of temperature and relative humidity in PEMFCs. To the best of our knowledge, this work is the first that evaluates the usability of functional textiles in continuous monitoring of energy devices. To this end, we fabricate thread-based sensors by the sequential coating of polyester threads with a CNT-based ink. The ability to pattern the sensors in a fuel cell is demonstrated by embroidering the sensors into a woven gas diffusion layer (GDL). The effect of the addition of the thread-based sensors to the GDL on the porous structure of the GDL is evaluated using microstructure analysis, scanning electron microscopy (SEM), and X-ray microtomography (X-μCT). We assessed the impact of thread-based sensors on the in-plane (IP) and through-plane (TP) electrical resistance, water transport, and overall performance of the fuel cell. Further, we investigate the widely neglected reciprocal effect of RH on temperature measurements by exploring different coating materials. Lastly, we showcase the ability of thread-based sensors in measuring spatiotemporal temperature variations in a model fuel cell.

RESULTS AND DISCUSSION

Integrating multifunctional threads within carbon cloth GDLs provides (1) preferential water "pathways" and (2) sensing capability within the fuel cell membrane electrode assembly (MEA). Figure 1a shows the process for sewing hydrophilic threads onto carbon cloth GDLs using a commercial sewing machine. Threads made of polyester, which has high wicking property compared to other commodity threads (see Figure S1), provided preferred pathways for water to cross the carbon

https://doi.org/10.1021/acsomega.0c06309
ACS Omega 2021, 6, 9509−9519

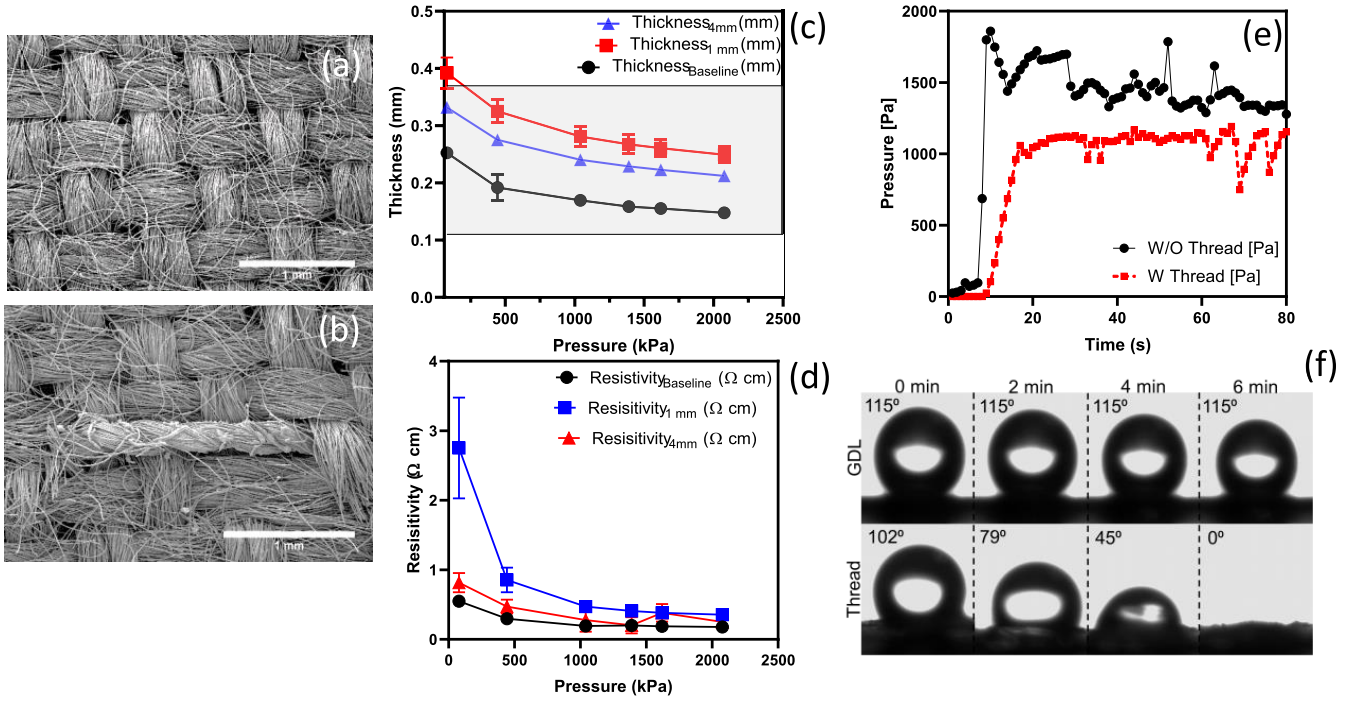

Figure 2. Investigating the effect of threads on the physical properties of GDLs. SEM images of a pristine carbon cloth GDL (a) and that with the hydrophilic thread (b) (scale bar is 1 mm). (c) Thickness under compression and (d) resistance under compression for a pristine carbon cloth, with 1 and 4 mm distances with 1 mm pitch distance of the hydrophilic thread. (e) Effect of the hydrophobic thread on the water breakthrough pressure. (f) Contact angle of the sessile water droplet on the carbon cloth GDL and the thread. Error bars represent standard deviation (SD) (n = 3).

cloth GDL (Figure 1a) with a minimal impact on the GDL microstructure. To add sensing within GDLs, the threads were functionalized by CNT to be temperature and humidity sensors. This requires a layer to insulate the CNT-coated thread from the conductive substrate (carbon cloth GDLs), as well as a protective layer to mitigate the sensitivity to humidity. The proposed low-cost process uses a roll-to-roll system to coat commodity threads with CNT inks by dipping and drying (Figure 1b). Poly(dimethylsiloxane) (PDMS) is an insulator with the high water vapor transmissivity required for RH sensitivity. PDMS can be easily wrapped around the CNT-coated thread via a dip-coating process. To achieve independent temperature sensitivity, fluorinated ethylene propylene (FEP) was used to coat the CNT-coated thread; this provides both insulation and mitigation of water vapor transmission (Figure 1c). The thread-based sensors monitor temperature and humidity locally and communicate wirelessly with a personal computer or smartphone. A schematic of sewing thread-based sensors on a piece of carbon cloth GDL is shown in Figure 1d. The detailed analysis of these integrated sensor-textile electrodes is presented in the following figure panels.

We evaluated the effect of the addition of threads on the physical properties of the GDL. A carbon cloth GDL has a plain weave of carbon yarns with a size of ~422 ± 3 μm. The SEM image in Figure 2a reveals the two-dimensional (2D) view of the microstructure of a plain GDL. A piece of polyester thread was treated with a corona discharge to enhance the wicking property of the thread (Figure S2 shows the wicking test results and Figure S3 the SEM images of the thread). The treated polyester thread with a diameter of ~232 ± 3 μm was sewed on a piece of cloth GDL, as depicted in Figure 2b. The SEM image showed that the thread was embedded in the pristine GDL with a minimal impact on the microstructure. For nonwoven GDLs, such as Toray 090, the microstructure was impacted, as shown in Figure S4. Threads were sewed in a straight line on a GDL with two patterns, 1 and 4 mm distance apart with a pitch of 1 mm. An in-house tool, thickness under compression and resistance under compression (TUC_RUC), was utilized to measure the thickness and through-plane electrical conductivity in different compression pressures. This tool has been used and evaluated in previous studies.[20,21] The thickness increased by ~100 μm for the 1 mm distance threaded GDL and 60 μm for the 4 mm one at 1500 kPa, which showed that the thickness of the modified GDL is in the range of commercial products (the gray area in Figure 2c, i.e., the thickness of these two commercial products are 370 μm for Toray 120 and 110 μm for Toray 030). On the other hand, electrical resistance under compression yields similar results compared to the pristine sample, even though the threads are nonconductive (Figure 2d). Another property is the effect of the thread on the water breakthrough pressure, i.e., the required pressure for water to penetrate a porous structure. This test was performed on pristine and threaded samples. The breakthrough pressure decreased ~30% for threaded GDLs (Figure 2e and the replicate in Figure S5). (However, the breakthrough pressure for a nonwoven GDL is zero due to significant structure alteration (Figure S6).) The reason for the lower breakthrough pressure might be due to a change in hydrophobicity of the structure rather than the sewing process. Hydrophobicity and contact angle were characterized using sessile drop tests. A water droplet was placed on the GDL, and the contact angle remained constant for over 6 min (115°); however, for a water droplet on the thread, the angle changed (from 101° to zero) and the droplet wicked through the polyester thread in 6 min (Figure 2f). This suggests that the

https://doi.org/10.1021/acsomega.0c06309
ACS Omega 2021, 6, 9509−9519

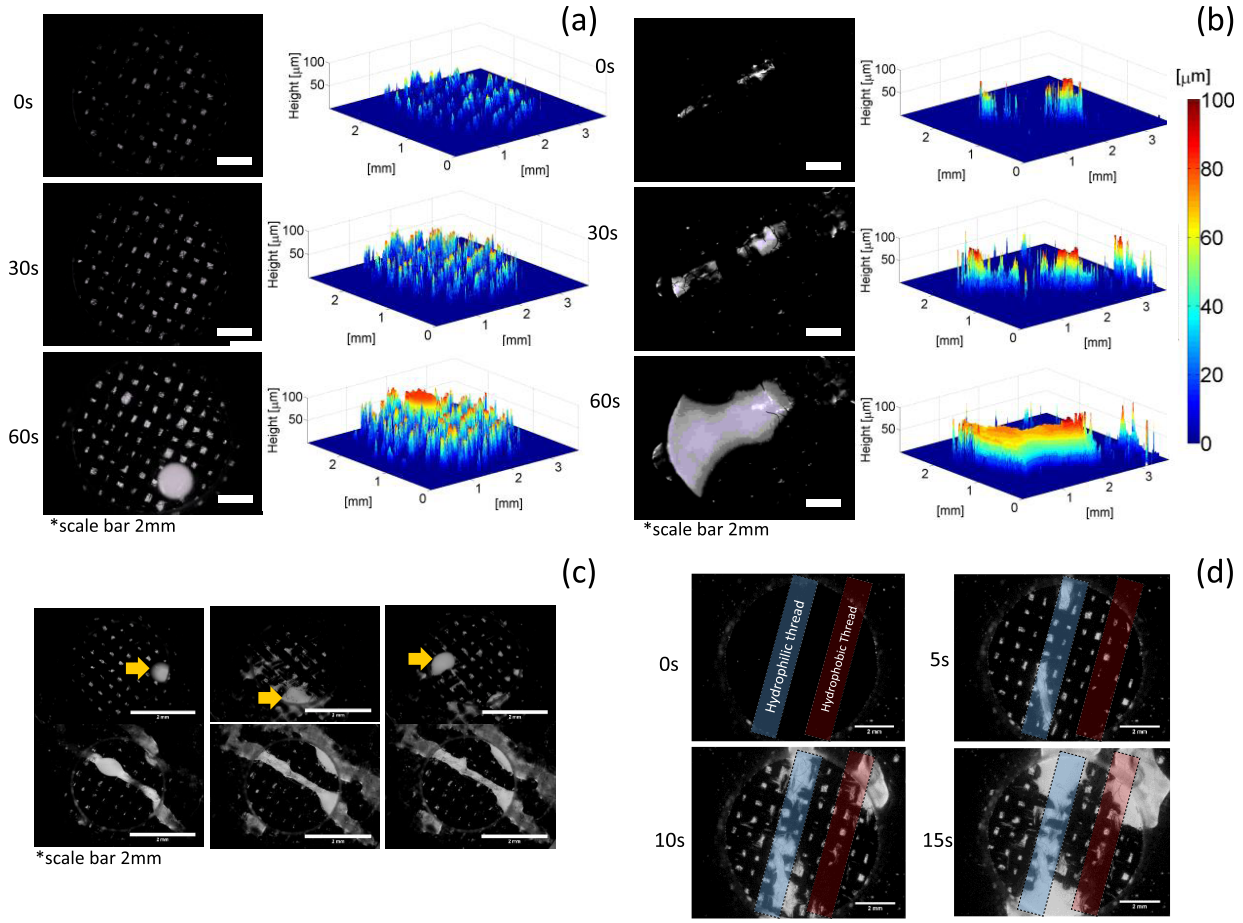

Figure 3. Water transport analysis via fluorescent microscopy. (a) Pristine carbon cloth and (b) with the thread. (c) Fixed water breakthrough location for the GDL with the thread and (d) the effect of hydrophobic and hydrophilic threads on the breakthrough.

thread wicking property can be used to develop water pathways within GDLs.

In this panel, we investigated the effectiveness of the thread in creating water transport pathways using fluorescent microscopy. High temporal resolution was used to track the dynamic water transport through the porous structure.[20] Figure 3a shows that water was first transported in the IP direction and filled the pores of the GDL, and, then, the breakthrough occurred; however, for the GDL with the thread, water was transported through the threaded regions with the remaining area available for eventual reactant transport, Figure 3b (Supporting videos 1 and 2 show the results). The 3D view of the water transport confirmed that the threaded area is the main pathway for water transport compared to the pristine sample. In addition, the breakthrough location remained fixed for the modified GDL, whereas for the pristine GDL, water transport occurred in three different locations (shown with yellow arrows) in three consecutive breakthrough tests (Figure 3c). The effect of thread hydrophobicity was also analyzed with the blue area corresponding to a hydrophilic thread (polyester) and the red area to a hydrophobic thread (carbon fiber yarn); both threads were sewed similarly on the substrate. The water breakthrough test showed that the hydrophilic region was wetted and that the hydrophobic thread did not show any sign of water. This indicates that the wetting properties are more important than the sewing process in determining the preferential water breakthrough location (Figure 3d). These results demonstrate that threads can be embedded in the structure of the GDL to effectively create water pathways.

The depth of the field of 2D SEM images limits observations to the inner layer of modified GDLs. Internal changes in microstructural properties were analyzed using X-μCT. High-resolution (voxel size of 3.16 μm) tomography resolves the pores and the 3D structure of the GDL, allowing for evaluation of the transport properties. Two pieces of the carbon cloth GDL with and without threads were scanned. The grayscale images consist of voxels with different grayscale values. The voxels of (1) pores were assigned to zero, (2) carbon fibers to one, and (3) the thread to two via a manual segmentation tool using Avizo software, which allows for generation of a 3D image of the substrate and segments in three different phases. The sample size with an area of 2.7 mm × 2.7 mm is shown in Figure 4a,b. One of the key properties is the bulk porosity, a fraction of pore volume to the total volume, which was found to drop by ∼5% compared to pristine samples (Figure 4c). The 3D image allows us not only to estimate the bulk porosity but also the variations of the porosity along any direction. The TP direction is shown in red, and the two IP directions perpendicular to TP are shown as blue and green axes in Figure 4a. For the sample with the stitch, the IP direction was separated into two parts: parallel to the thread ($IP_{parallel}$), blue, and perpendicular to the thread ($IP_{perpendicular}$), green. Because the thread direction imparts complete anisotropy, these two directions must be investigated separately. Porosity distributions in three main axes show the nonhomogeneity of the

https://doi.org/10.1021/acsomega.0c06309
ACS Omega 2021, 6, 9509−9519

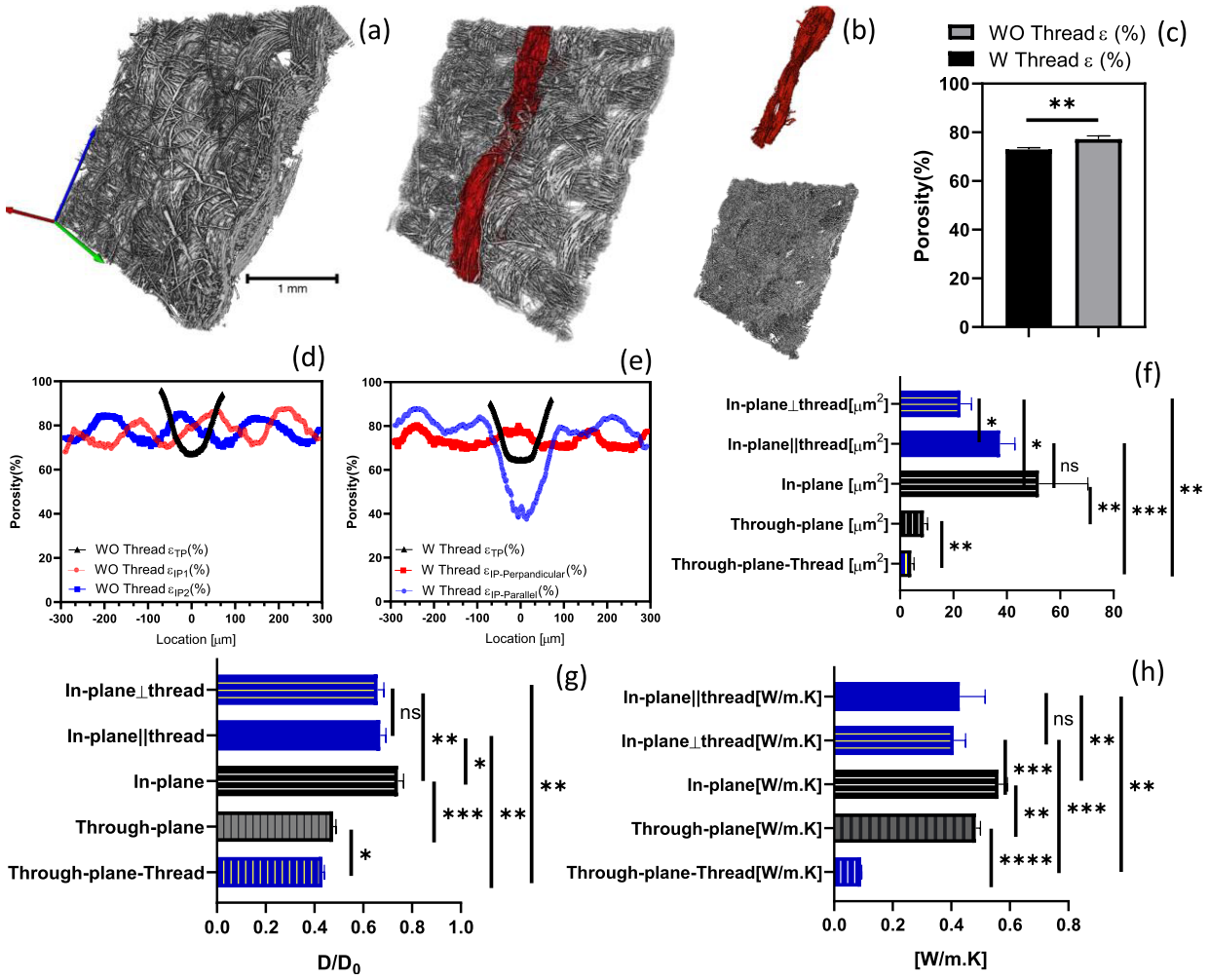

Figure 4. 3D microstructural analysis for evaluating transport properties. (a) X-μCT 3D images of the pristine GDL and (b) that with the hydrophobic thread; the thread and the carbon cloth are segmented (scale bar is 1 mm). (c) Change in bulk porosity due to the existing thread. (d) Porosity distribution for the pristine carbon cloth and (e) with the hydrophilic thread. Analysis of the effect of the thread on (f) diffusivity, (g) permeability, and (h) thermal conductivity (the pristine carbon cloth is black and that with the thread is blue). Error bars represent SD (n = 3); *ns = not significant, *p < 0.05, **p < 0.005, ***p < 0.0005, and **** p < 0.0001.

porous structure along different directions.[22] The TP and $IP_{perpendicular}$ directions of the threads show a similar trend of porosity distributions compared to the pristine sample (the black line (TP) and the red line ($IP_{perpendicular}$) graphs in Figure 4d,e). However, there is a sharp drop in the local porosity in the parallel-to-the-thread direction compared to the pristine sample (the blue line ($IP_{parallel}$) in Figure 4d,e). The porosity dropped ~40% locally in $IP_{parallel}$. This drop, however, is a location that is potentially filled with water during the fuel cell operation due to water wicking and is emitted in effective porosity estimation of the sample.[23] Although this location shows significant porosity changes locally, it could keep other pores available for reactant transport.

For the model based on X-μCT images, these properties were estimated using Avizo XLab.[24] This software solves continuum transport equations through a representative reconstructed porous domain.[25] The domain size that can be a representative volume element of the porous media was chosen to be 500 μm × 500 μm × thickness.[24,26] Since GDLs have an inhomogeneous structure, the permeations were measured in three main directions: TP, $IP_{parallel}$, and $IP_{perpendicular}$. The permeability measurement is based on Darcy's law. As expected from the literature,[27] the TP direction has lower permeability values than the IP directions. Introducing a thread reduced the permeation in the TP and the IP directions. In $IP_{perpendicular}$, the change was more significant (from 51.6 to 22.6 μm^2) relative to $IP_{parallel}$ (Figure 4f). The diffusivity was estimated based on Fick's law and found to be lower compared to the pristine GDL. It can be estimated that the molecular diffusion is less affected as a result of this modification (Figure 4g). Finally, the thermal conductivity was determined in similar steps. The thermal conductivity decreased with the introduction of the thread; however, there is no difference in $IP_{perpendicular}$ and $IP_{parallel}$ (Figure 4h). In summary, investigation of changes in the microstructural and transport properties shows that introducing threads for combined water management and sensing has a penalty of slightly lower but still acceptable transport properties compared to commercial products (i.e., Toray 090 permeability 10.5 μm^2 in IP and 3.5 μm^2 in TP and diffusivity 0.36 in TP and 0.63 in IP[24]).

We evaluated the trade-off between improved water transport and reduced transport properties by in situ testing of threaded GDLs in an operating fuel cell. A carbon cloth

https://doi.org/10.1021/acsomega.0c06309
ACS Omega 2021, 6, 9509−9519

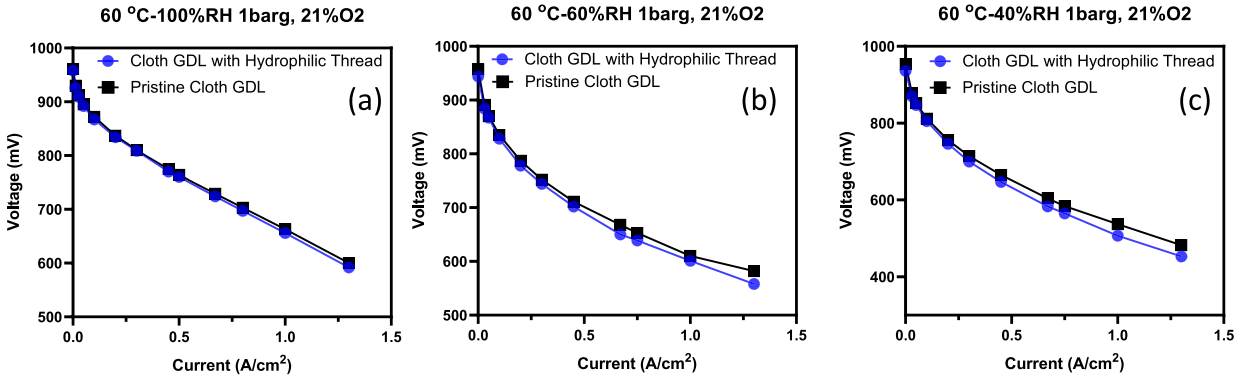

Figure 5. In situ fuel cell testing for the pristine carbon cloth GDL and the cloth GDL with the hydrophilic thread. The polarization curve at 60 °C and 21% O_2 for RH at (a) 100%, (b) 60%, and (c) 40%.

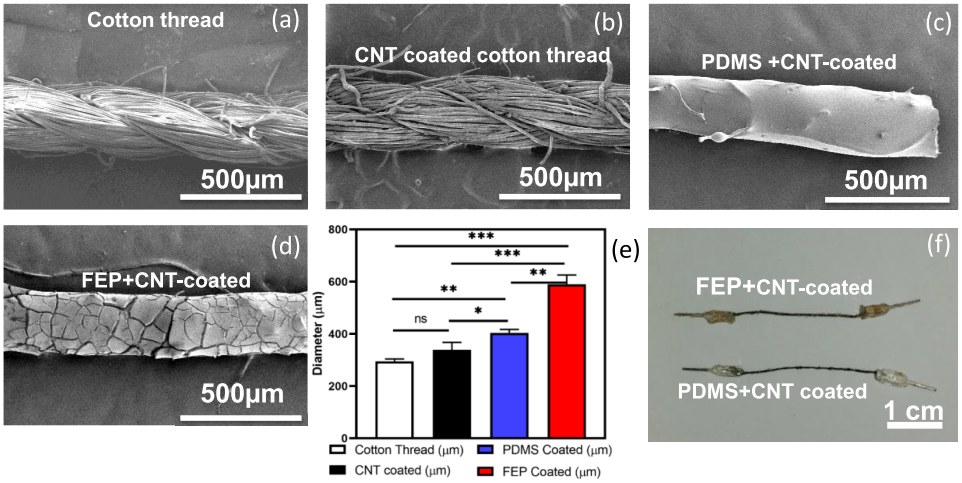

Figure 6. (a) Pristine, (b) CNT-coated, (c) CNT-coated with PDMS, and (d) CNT-coated with FEP cotton threads (scale bar 500 μm). (e) Change in the diameter after different coatings. (f) Optical images of thread-based sensors. Error bars represent SD ($n = 3$); *$p < 0.05$, **$p < 0.005$, and ***$p < 0.0005$.

GDL with a thread 4 mm apart, parallel to the flow field channel, was located on the cathode side where water management was more crucial. A pristine carbon cloth GDL was placed on the anode side to obtain an MEA and compare the results with an MEA with pristine woven GDLs on both sides. Figure 5a–c shows the polarization curve of the threaded MEA (blue line) and the pristine MEA (black line). The tests were performed at three different RH values (100, 60, and 40% at 60 °C). At high RH, the performance of both MEAs is similar. However, at low RH, the pristine sample exhibited better performance; this is expected as excess water/flooding does not typically occur under low RH conditions. The in situ testing indicated that the usage of the thread did not drastically alter the fuel cell performance in various conditions. This shows the potential capability of introducing sensing threads for monitoring temperature and humidity with minimal adverse effects on the performance of PEMFCs.

In previous experiments, we showed that threaded GDLs do not reduce the fuel cell performance, and we next investigated sensing threads that can monitor temperature and humidity locally. Sensing was achieved by coating a cotton thread (Figure 6a) with CNT ink (functionalized multiwalled carbon nanotubes (fMWCNTs) with sodium dodecyl sulfate (SDS) dissolved in distilled water) (Figure 6b). The CNT-coated thread shows stable conductivity for over six months (Figure S7). The key properties of fMWCNTs for this application are (1) conductivity and (2) sensitivity to both temperature[16] and humidity.[28] The resistance of the CNT-coated substrate changed according to temperature and humidity changes, as reported in previous studies that used the sensing property of CNTs for either temperature or humidity monitoring. Since both parameters can vary simultaneously in an operating fuel cell, the signals have to be segregated. This requires a coating that (1) insulates from a conductive substrate (e.g., carbon cloth), (2) mitigates the response to humidity changes, and (3) is flexible enough to be sewn on a substrate. PDMS, a flexible polymer that can easily coat a variety of substrates, was used to provide a thin insulating layer around the thread (Figure 6c). PDMS also has a high water vapor transmission rate and therefore does not inhibit RH sensing with CNT-coated threads. For temperature sensing, FEP was used to stop/reduce RH sensitivity. FEP is a hydrophobic polymer that increases the hydrophobicity of a GDL,[2] has a low water vapor transmission rate, and also has sufficient flexibility to be sewed on a substrate. The CNT-coated thread was coated with a 55 wt % FEP solution (Figure 6d). Each coat (PDMS and FEP) increased the diameter of the thread. In this work, a cotton thread with a diameter of 350 μm was used. After PDMS coating, the diameter increased to 400 μm, and with FEP coating, it increased to 590 μm (Figure 6e). This can be easily tuned by choosing a thread with a different initial diameter. Figure 6f shows two sensing threads.

https://doi.org/10.1021/acsomega.0c06309
ACS Omega 2021, 6, 9509−9519

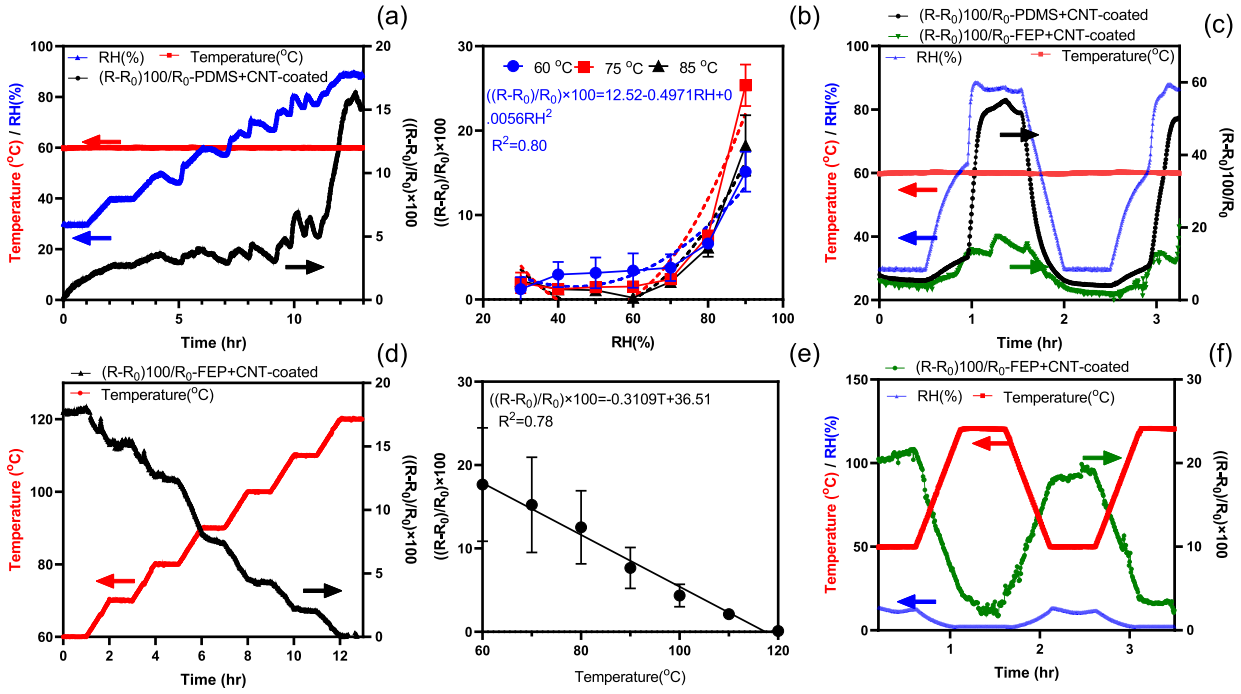

Figure 7. (a) Capturing the response of the sensor in changing RH values from 30 to 90%. (b) Sensor response for three different temperatures with varying RHs. (c) Stepwise response of the sensor between 30 and 90% RH changes. (d) Capturing the response of the sensor on changing temperature values from 60 to 120 °C. (e) Sensor response with varying temperatures. (f) Stepwise response of the sensor between 50 and 120 °C. Error bars represent SD (n = 3).

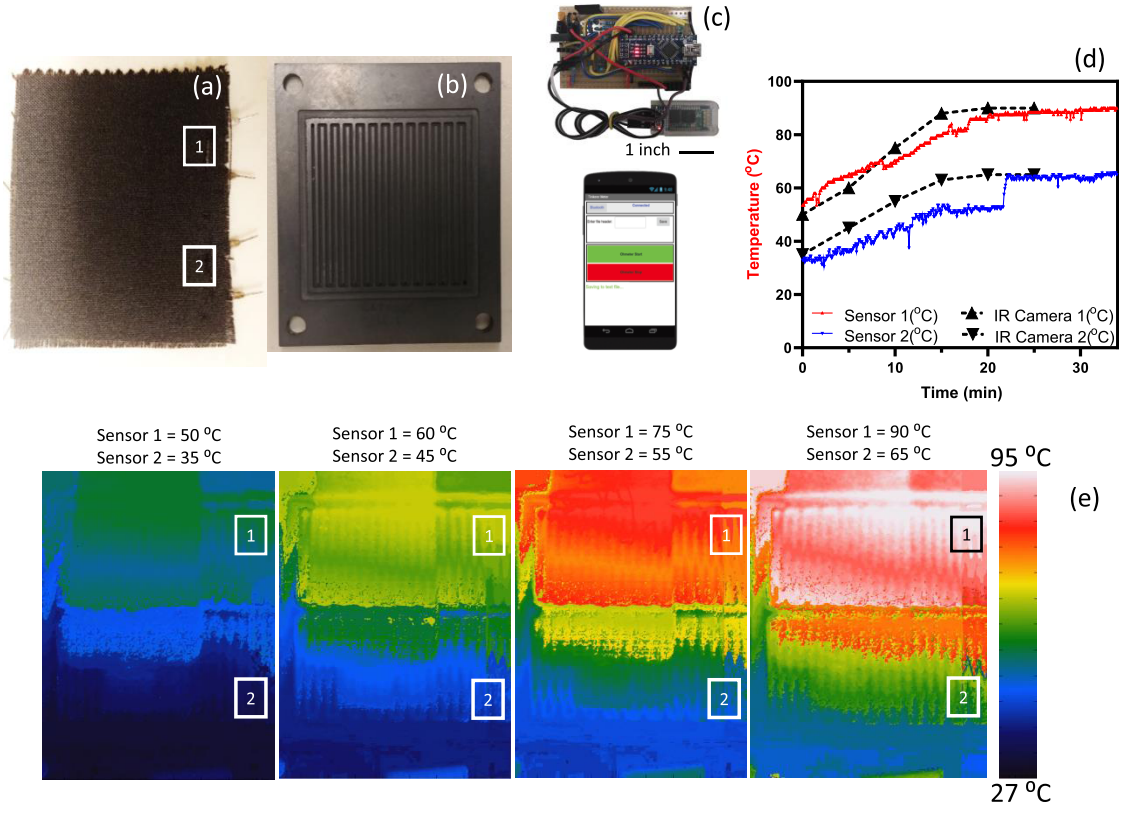

Figure 8. (a) Carbon cloth GDL with two temperature sensors sewed and placed on (b) a flow field and (c) a circuit board communicating with a smartphone. (d) Temperature monitoring via sensors (red and blue for locations 1 and 2, respectively) and the black line via a thermal camera. (e) Temperature map over half an hour of nonhomogeneous temperature distributions.

To analyze the response of both sensors, three samples (3 cm long threads) of (1) PDMS + CNT-coated and (2) FEP + CNT-coated were prepared and tested in an environmental chamber. The testing conditions were similar to those in a

https://doi.org/10.1021/acsomega.0c06309
ACS Omega 2021, 6, 9509−9519

typical fuel cell (60 °C and RH varying between 30 and 90%). The measurements were performed after steady-state conditions were reached in the environmental chamber (half an hour for each state and half an hour for the ramping time). The resistance of the threads was monitored at 20 s intervals. The environmental chamber was programmed to change the RH from 30 to 90% for over 13 h. The resistance of the PDMS-coated thread (black line) followed the pattern of the RH curve (blue line) (Figure 7a). The change of the resistance of the thread was more sensitive at high RH values (more than 60% RH), which is critical for PEMFC application since the membrane of fuel cells always needs to be hydrated.[29] The test was repeated at 75 and 85 °C. It was shown that the thread resistance followed a quadratic function of RH. A similar pattern was observed for all three temperatures with slightly higher sensitivity at 75 °C. The sensitivity of the thread between 30 and 70% was low compared to higher humidity levels. Also, the variations between different samples might be associated with the dip-coating procedure of CNT and PDMS on the thread (Figure 7b). Figure 7c shows that the resistance of PDMS + CNT-coated threads followed the RH cycle (blue line) at constant temperature (red line). However, the resistance of FEP + CNT-coated threads showed a small change with large RH changes (less than 15%). The PDMS + CNT-coated thread resistance showed the same trend for repeated cycles over a 7 h test cycle (Figure S8). The tests were repeated three times for each condition and a similar pattern with a variation of 4.5% was observed as shown in Figure S9. This indicates that FEP coating can mitigate the RH response of the CNT-coated thread and can be used solely to monitor temperature, while PDMS + CNT-coated threads can be used for RH sensing.

The temperature response of FEP + CNT-coated threads characterized by varying the temperature between 50 and 120 °C in steps (with an increase of 10 °C, ramping time of 1 h, and steady time of 1 h and R_0 is 29 kΩ/cm). Figure 7d shows the stepwise decrease in resistance of the thread with increasing temperature. The linear graph of the thread resistance vs temperature (with the slope of ∼−0.31%/°C) is illustrated in Figure 7e. The thread-based temperature sensor response was also characterized by rapid temperature cycling from 50 to 120 °C. The resistance varied inversely with temperature and returned to the initial resistance with no hysteresis. The tests showed good repeatability (Figure 7f). The combination of both PDMS + CNT-coated and FEP + CNT-coated threads can be embedded in a textile GDL in an operating fuel cell for mapping temperature and humidity locally.

To showcase the feasibility of the proposed approach and provide proof of the concept, two pieces of thread-based temperature sensors (FEP + CNT-coated) were sewed on a piece of carbon cloth GDL to monitor the temperature of the substrate locally (Figure 8a). The modified GDL was placed on a flow field (Figure 8b) and then exposed to nonuniform heat, which was generated by a hot plate, to develop a nonuniform temperature distribution across the GDL. The sample was then monitored by an infrared (IR) camera for over 30 min. Four snapshots from the IR camera indicated the temperature distributions from 27 up to 95 °C. The two temperature sensor locations are indicated by "1" and "2." The resistance of the threads was monitored wirelessly via an in-house circuit board that communicated with a smartphone (Figure 8c). The resistance was correlated to the temperature based on a linear decrease in the value. The sensors monitored the temperature increase from 50 to 90 °C and 35 to 65 °C for locations 1 and 2, respectively. On the other hand, the temperature was captured via an IR camera and compared with thread-based temperature sensors. Six time points were chosen for comparison between these two measurement methods, exhibiting a good agreement between the IR camera results and the thread-based temperature sensors (Figure 8d). The temperature maps at four time points are depicted in Figure 8e. These results indicated that the thread-based sensors can easily map temperature on a textile electrode.

CONCLUSIONS

In this work, we developed an integrated approach for sensing and water management in fuel cells that uses functionalized threads. Selective hydrophilic pathways were generated within the porous structure of an electrode through a low-cost sewing process. The microstructural analysis showed that external threads embedded within the GDL have minimal impact on transport properties. In situ fuel cell testing showed that the impact on the overall performance is minimal when enhancing water management at the expense of reducing transport properties.

Furthermore, cotton threads were transformed into humidity and temperature sensors by incorporating CNTs into cotton yarns with two separate protective layers (PDMS for the humidity sensor and FEP for the temperature sensor). The thread-based humidity sensors showed a quadratic resistance increase to the change of RH (between 60 and 90%), while temperature sensors showed a linear resistance decrease to the change of temperature (between 50 and 120 °C).

These sensors can be embedded into the textile electrode for monitoring temperature and RH locally without compromising fuel cell performance. Ex situ temperature monitoring was performed on a carbon cloth GDL with a nonhomogeneous temperature distribution, which proved the functionality of the sensors. This study indicates that textile electrodes in electrochemical devices, specifically fuel cells, can be modified to control the transport of byproducts, i.e., water, and also to monitor local parameters, i.e., temperature and RH, by adding sensing yarn to textile electrodes. Besides, they have potential applications in flexible and wearable textile batteries.[30−33]

EXPERIMENTAL SECTIONS

Materials. The woven GDL, AvCarb 1071 HCB, nonwoven GDL, Toray 090, and fluorinated ethylene propylene (FEP) (FEPD121 DuPont 55% solids) were purchased from Fuelcell Earth, and functionalized multiwalled carbon nanotubes (fMWCNTs), sodium dodecyl sulfate (SDS), and rhodamine B were purchased from Sigma-Aldrich.

Microscopy. Scanning electron microscopy (SEM) images were captured using a Hitachi S-4800N scanning electron microscope. Fluorescent microscopy was performed using an upright fluorescent microscope (DP 73 Olympus BX51), with a CY3 filter and 2× objective and a numerical aperture (NA) of 0.06 to observe water transport. The contact angle of a sessile drop of distilled water was measured using a goniometer from DataPhysics (model TBU 90E).

Fluorescent Visualization and Breakthrough Pressure. The water breakthrough pressure was measured using a differential pressure transducer (Honeywell FP2000) with a

https://doi.org/10.1021/acsomega.0c06309
ACS Omega 2021, 6, 9509−9519

data acquisition system. Following our previous study,[20] a syringe pump was used to inject a dilute distilled water solution of 1 mM rhodamine B (excitation: 540 nm and emission: 635 nm) with a rate of 0.02 mL/min into the apparatus. The water height is correlated to the intensity of the image since the depth of the field is calculated using $d_{field} = \lambda/NA^2$, which is 150 μm, and due to the porous structure, the depth of the field is up to 7−8 fibers, which is ∼100 μm. As a result, the height is calculated using $\eta = \frac{100}{255} I[\mu m]$, where η is the observable height and I is the intensity of the image. The field of view is 6.5 mm × 5 mm, and the resolution is 4.6 μm. Details of the imaging are provided in ref 20.

Thickness and Electrical Conductivity Measurements. A custom-made testbed (known as thickness under compression−resistivity under compression, TUC_RUC) was used to measure the sample thickness and the through-plane resistivity at various pressures. A sample was clamped between two gold-plated probes. To cancel the electrical contact resistance (ECR) between plates and GDLs, the testing of different thicknesses was required, which was achieved by stacking GDLs. By subtracting two stacks, ECRs between the probes and the GDL surfaces were mitigated, and since the ECR in stacked GDLs is negligible, the obtained value is the GDL resistivity, as shown in previous studies.[20,23]

X-μCT Imaging. X-ray microtomography (X-μCT) was performed using a Zeiss MIcroXCT-400 machine at UBC Okanagan. A 5 mm × 5 mm sample was cut and secured to the sample holder. It was glued to avoid fluttering during movement. Then, 2500 radiograph images were obtained by spanning 360° with an exposure of 15 s. A 4× objective lens was used to acquire a spatial resolution of 3.16 μm for each micrograph. Image processing was performed using ImageJ, MATLAB, and Avizo software, followed by reconstructing the 2D slices from the scans. First, a median filter with a kernel size of 2 was applied on grayscale images to reduce the noise, then manual thresholding was performed to segment the materials from the background. To segment the thread from the substrate, the segmentation module of Avizo was used to manually separate the thread from the GDL for subsequent transport properties' analysis.

Transport Properties' Estimation. The bulk porosity and porosity distribution were obtained by calculating the porosity in each 2D radiograph. The details of the procedure can be obtained from refs 34, 35. For the permeability analysis, Darcy's law was employed via the absolute permeability experiment simulation tool within the Avizo XLab module with a convergence criterion 10^{-6}. Molecular diffusivity following Fick's second law was solved with the molecular diffusivity experiment simulation tool within the Avizo XLab module, and thermal conductivity simulation was performed with the Avizo XLab thermal conductivity module.

In Situ Fuel Cell Testing. A single cell with an MEA size of 90 mm × 50 mm and a flow field with a channel size of 1.1 mm and landing of 0.21 mm were used for the test. The temperature was set to 60 °C. The RH in the anode was set to 100%, and the RH in the cathode varied between 40 and 100%. A catalyst-coated membrane (CCM), Ballard CCM with 30 wt % Nafion and 0.1 and 0.4 mg/cm^2 Pt loading on the anode and the cathode, respectively, was used. The control MEA had two carbon cloths (Avcarb 1071 HCB) on both the cathode and the anode sides. The carbon cloth (Avcarb 1071 HCB) with a thread sewed (polyester thread) 4 mm apart was used in the cathode side of the MEA, and on the anode side, a pristine GDL was used.

Preparation of CNT Ink. Briefly, 1.6 mg/mL fMWCNT and 10 mg/mL SDS were dispersed in distilled water with 1 min probe sonication to obtain a well-dispersed solution.

Preparation of CNT-Coated Cotton Threads. A commodity thread was first corona-discharged to enhance the wetting property. Then, it was dipped-coated six times and dried in an oven at 80 °C for half an hour for each dipping.

FEP and PDMS Coating of CNT-Coated Threads. A CNT-coated thread was dipped into a 55% FEP solution, followed by demoisturization at 100 °C in a hot plate. Subsequently, it was heated up to 300 °C in order for sintering FEP onto the thread. The CNT-coated threads were dipped into PDMS (10:1 ratio of PDMS and the curing agent) and dried on a hot plate at 90 °C for 2 h.

Temperature and Relative Humidity Measurements. The temperature and humidity were controlled by an environmental chamber (TestEquity model 123H). Three pieces of thread-based sensors were placed in the chamber, and the resistance was monitored using an in-house board.

Wireless Monitoring of Temperature. Two off-the-shelf components, the Arduino Nano Every and the HC-06 Class 2 Slave Bluetooth module, were used for data processing and transmission. For separate and simultaneous measurements of the surrounding environment's temperature and humidity, the output voltages of the two electrodes were logged by an Arduino (SparkFun, Niwot, CO) microcontroller with a 1 kHz sampling frequency. A voltage divider circuit with an applied 5 V voltage source and known R_1 resistor values was employed to determine the resistance of the electrode, R_2, via thresholding of the resulting analog output voltage. To reduce the error in measurement of the output voltage, a range of resistor values (100−10 MΩ) was used to compare against the unknown electrode resistance in the voltage divider. The calculated electrode resistance data was then sent to an HC-06 (DSD TECH) wireless serial Bluetooth module and then transmitted to a mobile phone. A custom Android app allowed for the continuous collection of temperature and humidity conditions. Electrode resistance measurements were updated every 5 s.

IR Camera. A thermal camera (Seek Thermal-Compact) was used to map the temperature distribution. It monitored the change of temperature over a 30 min test.

■ ASSOCIATED CONTENT

Supporting Information

The Supporting Information is available free of charge at https://pubs.acs.org/doi/10.1021/acsomega.0c06309.

Wicking test for three commercial threads (after the corona discharge treatment), thread wetting following a square root of time and the polyester thread showing the highest wicking property (Figure S1); effect of the corona discharge on the wicking property of the polyester thread (Figure S2); effect of the corona discharge on the microstructure of the thread (a) before treatment and (b) after treatment (Figure S3); effect of sewing the thread on the nonwoven GDL (Toray 090) (Figure S4); two replicates of the breakthrough pressure for the carbon cloth GDL with and without the thread in (a) and (b) (Figure S5); effect of sewing the thread on the breakthrough pressure of the nonwoven GDL vs the

https://doi.org/10.1021/acsomega.0c06309
ACS Omega 2021, 6, 9509−9519

pristine nonwoven GDL (Figure S6); resistance of the 3 cm long CNT-coated thread for over six months (the number of samples is 3) (Figure S7); cyclic response to RH changes of the thread-based RH sensor (PDMS +CNT-coated) (Figure S8); and cyclic RH response for three replicates of thread-based temperature and RH sensors (Figure S9) (PDF)

Video S1: Water transported in pristine carbon cloth GDL (AVI)

Video S2: Water transported in carbon cloth GDL with hydrophilic thread (AVI)

AUTHOR INFORMATION

Corresponding Authors

Mohsen Akbari − *Laboratory for Innovations in Microengineering (LiME), Department of Mechanical Engineering, University of Victoria, Victoria, British Columbia V8P 5C2, Canada; Biotechnology Center, Silesian University of Technology, 44-100 Gliwice, Poland;* orcid.org/0000-0003-2902-6557; Email: makbari@uvic.ca

Ned Djilali − *Department of Mechanical Engineering and Institute for Integrated Energy System, University of Victoria, Victoria, British Columbia V8W 3P6, Canada; Institute of Engineering Thermophysics, School of Energy and Power Engineering, Chongqing University, Chongqing 400030, China*; Email: ndjilali@uvic.ca

Authors

Sadegh Hasanpour − *Laboratory for Innovations in Microengineering (LiME), Department of Mechanical Engineering and Department of Mechanical Engineering and Institute for Integrated Energy System, University of Victoria, Victoria, British Columbia V8P 5C2, Canada*

Armin Rashidi − *Composites Research Network-Okanagan Node (CRN), School of Engineering, University of British Columbia, Kelowna, British Columbia V1V 1V7, Canada*

Tavia Walsh − *Laboratory for Innovations in Microengineering (LiME), Department of Mechanical Engineering, University of Victoria, Victoria, British Columbia V8P 5C2, Canada*

Erik Pagan − *Laboratory for Innovations in Microengineering (LiME), Department of Mechanical Engineering, University of Victoria, Victoria, British Columbia V8P 5C2, Canada*

Abbas S. Milani − *Composites Research Network-Okanagan Node (CRN), School of Engineering, University of British Columbia, Kelowna, British Columbia V1V 1V7, Canada*

Complete contact information is available at: https://pubs.acs.org/10.1021/acsomega.0c06309

Notes

The authors declare no competing financial interest.

ACKNOWLEDGMENTS

This research was supported by the Natural Sciences and Engineering Research Council of Canada and the Canadian Institutes for Health Research. The authors thank Ballard Power Systems for providing access to experimental testing facilities.

REFERENCES

(1) Chu, S.; Majumdar, A. Opportunities and Challenges for a Sustainable Energy Future. *Nature* **2012**, *488*, 294−303.

(2) Forner-Cuenca, A.; Biesdorf, J.; Gubler, L.; Kristiansen, P. M.; Schmidt, T. J.; Boillat, P. Engineered Water Highways in Fuel Cells: Radiation Grafting of Gas Diffusion Layers. *Adv. Mater.* **2015**, *27*, 6317−6322.

(3) Forner-Cuenca, A.; Penn, E. E.; Oliveira, A. M.; Brushett, F. R. Exploring the Role of Electrode Microstructure on the Performance of Non-Aqueous Redox Flow Batteries. *J. Electrochem. Soc.* **2019**, *166*, A2230−A2241.

(4) Flox, C.; Skoumal, M.; Rubio-Garcia, J.; Andreu, T.; Morante, J. R. Strategies for Enhancing Electrochemical Activity of Carbon-Based Electrodes for All-Vanadium Redox Flow Batteries. *Appl. Energy* **2013**, *109*, 344−351.

(5) Zhang, L.; Tarascon, J.-M.; Sougrati, M. T.; Rousse, G.; Chen, G. Influence of Relative Humidity on the Structure and Electrochemical Performance of Sustainable LiFeSO 4 F Electrodes for Li-Ion Batteries. *J. Mater. Chem. A* **2015**, *3*, 16988−16997.

(6) Guo, Z.; Dong, X.; Yuan, S.; Wang, Y.; Xia, Y. Humidity Effect on Electrochemical Performance of Li−O2 Batteries. *J. Power Sources* **2014**, *264*, 1−7.

(7) Wang, S.; Li, K.; Tian, Y.; Wang, J.; Wu, Y.; Ji, S. Infrared Imaging Investigation of Temperature Fluctuation and Spatial Distribution for a Large Laminated Lithium−ion Power Battery. *Appl. Therm. Eng.* **2019**, *152*, 204−214.

(8) Zou, D.; Liu, X.; He, R.; Zhu, S.; Bao, J.; Guo, J.; Hu, Z.; Wang, B. Preparation of a Novel Composite Phase Change Material (PCM) and Its Locally Enhanced Heat Transfer for Power Battery Module. *Energy Convers. Manag.* **2019**, *180*, 1196−1202.

(9) Jian, Q.; Zhao, J. Experimental Study on Spatiotemporal Distribution and Variation Characteristics of Temperature in an Open Cathode Proton Exchange Membrane Fuel Cell Stack. *Int. J. Hydrogen Energy* **2019**, *44*, 27079−27093.

(10) David, N. A.; Wild, P. M.; Jensen, J.; Navessin, T.; Djilali, N. Simultaneous In Situ Measurement of Temperature and Relative Humidity in a PEMFC Using Optical Fiber Sensors. *J. Electrochem. Soc.* **2010**, *157*, B1173−B1179.

(11) Nascimento, M.; Novais, S.; Ding, M. S.; Ferreira, M. S.; Koch, S.; Passerini, S.; Pinto, J. L. Internal Strain and Temperature Discrimination with Optical Fiber Hybrid Sensors in Li-Ion Batteries. *J. Power Sources* **2019**, *410−411*, 1−9.

(12) Shafiq, Y.; Gibson, J. S.; Kim, H.; Ambulo, C. P.; Ware, T. H.; Georgakopoulos, S. V. A Reusable Battery-Free RFID Temperature Sensor. *IEEE Trans. Antennas Propag.* **2019**, *67*, 6612−6626.

(13) Zhang, G.; Ge, S.; Xu, T.; Yang, X.-G.; Tian, H.; Wang, C.-Y. Rapid Self-Heating and Internal Temperature Sensing of Lithium-Ion Batteries at Low Temperatures. *Electrochim. Acta* **2016**, *218*, 149−155.

(14) Lee, C.-Y.; Peng, H.-C.; Lee, S.-J.; Hung, I.; Hsieh, C.-T.; Chiou, C.-S.; Chang, Y.-M.; Huang, Y.-P. A Flexible Three-in-One Microsensor for Real-Time Monitoring of Internal Temperature, Voltage and Current of Lithium Batteries. *Sensors* **2015**, *15*, 11485−11498.

(15) Lee, C.-Y.; Lee, S.-J.; Hung, Y.-M.; Hsieh, C.-T.; Chang, Y.-M.; Huang, Y.-T.; Lin, J.-T. Integrated Microsensor for Real-Time Microscopic Monitoring of Local Temperature, Voltage and Current inside Lithium Ion Battery. *Sens. Actuators, A* **2017**, *253*, 59−68.

(16) Mostafalu, P.; Akbari, M.; Alberti, K. A.; Xu, Q.; Khademhosseini, A.; Sonkusale, S. R. A Toolkit of Thread-Based Microfluidics, Sensors, and Electronics for 3D Tissue Embedding for Medical Diagnostics. *Microsystems Nanoeng.* **2016**, *2*, No. 16039.

(17) Mousavi, M. P. S.; Ainla, A.; Tan, E. K. W.; Abd El-Rahman, M. K.; Yoshida, Y.; Yuan, L.; Sigurslid, H. H.; Arkan, N.; Yip, M. C.; Abrahamsson, C. K.; et al. Ion Sensing with Thread- Based Potentiometric Electrodes. *Lab Chip* **2018**, *18*, 2279−2290.

(18) Owyeung, R. E.; Terse-Thakoor, T.; Rezaei Nejad, H.; Panzer, M. J.; Sonkusale, S. R. Highly Flexible Transistor Threads for All-Thread Based Integrated Circuits and Multiplexed Diagnostics. *ACS Appl. Mater. Interfaces* **2019**, *11*, 31096−31104.

(19) Wang, S.; Ye, D.; Liu, Z.; Chen, R.; Zhu, X.; Zhang, B.; Wu, R.; Liao, Q. A Direct Formate Microfluidic Fuel Cell with Cotton

Thread-Based Electrodes. *Int. J. Hydrogen Energy* **2020**, *45*, 27665−27674.
(20) Hasanpour, S.; Ahadi, M.; Bahrami, M.; Djilali, N.; Akbari, M. Woven Gas Diffusion Layers for Polymer Electrolyte Membrane Fuel Cells: Liquid Water Transport and Conductivity Trade-Offs. *J. Power Sources* **2018**, *403*, 192−198.
(21) Malekian, A.; Salari, S.; Tam, M.; Oldknow, K.; Djilali, N.; Bahrami, M. Compressive Behaviour of Thin Catalyst Layers. Part I - Experimental Study. *Int. J. Hydrogen Energy* **2019**, *44*, 18450−18460.
(22) Fishman, Z.; Hinebaugh, J.; Bazylak, A. Microscale Tomography Investigations of Heterogeneous Porosity Distributions of PEMFC GDLs. *J. Electrochem. Soc.* **2010**, *157*, B1643−B1650.
(23) Flückiger, R.; Marone, F.; Stampanoni, M.; Wokaun, A.; Büchi, F. N. Investigation of Liquid Water in Gas Diffusion Layers of Polymer Electrolyte Fuel Cells Using X-Ray Tomographic Microscopy. *Electrochim. Acta* **2011**, *56*, 2254−2262.
(24) Hasanpour, S.; Hoorfar, M.; Phillion, A. B. Characterization of Transport Phenomena in Porous Transport Layers Using X-Ray Microtomography. *J. Power Sources* **2017**, *353*, 221−229.
(25) Lange, K. J.; Sui, P.-C.; Djilali, N. Pore Scale Simulation of Transport and Electrochemical Reactions in Reconstructed PEMFC Catalyst Layers. *J. Electrochem. Soc.* **2010**, *157*, B1434.
(26) García-Salaberri, P. A.; Zenyuk, I. V.; Shum, A. D.; Hwang, G.; Vera, M.; Weber, A. Z.; Gostick, J. T. Analysis of Representative Elementary Volume and through-Plane Regional Characteristics of Carbon-Fiber Papers: Diffusivity, Permeability and Electrical/thermal Conductivity. *Int. J. Heat Mass Transfer* **2018**, *127*, 687−703.
(27) Gostick, J. T.; Fowler, M. W.; Pritzker, M. D.; Ioannidis, M. A.; Behra, L. M. In-Plane and through-Plane Gas Permeability of Carbon Fiber Electrode Backing Layers. *J. Power Sources* **2006**, *162*, 228−238.
(28) Zhou, G.; Byun, J. H.; Oh, Y.; Jung, B. M.; Cha, H. J.; Seong, D. G.; Um, M. K.; Hyun, S.; Chou, T. W. Highly Sensitive Wearable Textile-Based Humidity Sensor Made of High-Strength, Single-Walled Carbon Nanotube/Poly(vinyl Alcohol) Filaments. *ACS Appl. Mater. Interfaces* **2017**, *9*, 4788−4797.
(29) Wu, J.; Yuan, X. Z.; Martin, J. J.; Wang, H.; Zhang, J.; Shen, J.; Wu, S.; Merida, W. A Review of PEM Fuel Cell Durability: Degradation Mechanisms and Mitigation Strategies. *J. Power Sources* **2008**, *184*, 104−119.
(30) Huang, Q.; Wang, D.; Zheng, Z. Textile-Based Electrochemical Energy Storage Devices. *Adv. Energy Mater.* **2016**, *6*, No. 1600783.
(31) Huang, X.; Liu, J.; Ding, J.; Deng, Y.; Hu, W.; Zhong, C. Toward Flexible and Wearable Zn-Air Batteries from Cotton Textile Waste. *ACS Omega* **2019**, *4*, 19341−19349.
(32) Liu, M.; Pu, X.; Cong, Z.; Liu, Z.; Liu, T.; Chen, Y.; Fu, J.; Hu, W.; Wang, Z. L. Resist- Dyed Textile Alkaline Zn Microbatteries with Significantly Suppressed Zn Dendrite Growth. *ACS Appl. Mater. Interfaces* **2019**, *11*, 5095−5106.
(33) Ahadi, M.; Tam, M.; Saha, M. S.; Stumper, J.; Bahrami, M. Thermal Conductivity of Catalyst Layer of Polymer Electrolyte Membrane Fuel Cells: Part 1 − Experimental Study. *J. Power Sources* **2017**, *354*, 207−214.
(34) Hasanpour, S. Characterization of Porous Transport Layers of Polymer Electrolyte Membrane Fuel Cells Using X-Ray Micro-Computed Tomography. M.S. Thesis, The University of British Columbia, Kelowna, Canada, 2016.
(35) Hasanpour, S.; Hoorfar, M.; Phillion, A. B. Different Methods for Determining Porosity of Gas Diffusion Layer Using X-Ray Microtomography. *Electrochim. Acta* **2015**, *185*, 34−39.

https://doi.org/10.1021/acsomega.0c06309
ACS Omega 2021, 6, 9509−9519